

MAGNETOHYDRODYNAMIC MODELING OF CORONAL STRUCTURE AND EXPANSION

S. T. Suess+
Space Environment Laboratory
NOAA / ERL
325 Broadway
Boulder, Colorado 80303

ABSTRACT

The presence of a magnetic field in the corona adds structure to the solar wind and almost certainly plays an important role in the energetics of the flow. Here I will discuss analytical and numerical modeling of gas-magnetic field interactions as used to compute steady, global flow. After a brief and incomplete review, I will describe the approach used in, and results from a recent global model (Steinolfson, Suess and Wu, 1982). I will then outline my own ideas on the most effective ways to improve the physical content and numerical efficiency of these models. Throughout, I will limit myself to discussing solutions of the MHD equations only in order to find steady-state flows, even though this will often entail solving time-dependent equations.

INTRODUCTION

One of the more difficult problems in coronal dynamics is to self-consistently compute the large-scale interactions between the plasma and the magnetic field in order to find the flow geometry. The theoretical models that have been published generally either incorporate very important approximations in order to make the analysis tractable, or use "brute force" numerical solutions. As an example of an essentially analytic approach to MHD modeling, I describe the results from a quasi-radial flow approximation (Suess, Richter, Winge and Nerney, 1977; Suess, 1979; Winge and Coleman, 1974; Nerney and Suess, 1975; Suess, 1972). This approximation invoked flow that was nearly radial, deriving conditions for this requirement as a result from the analysis. Single-fluid, polytropic flow with no dissipation was assumed, and the flow was taken to be axisymmetric. The geometrical approximation means that the analysis cannot be applied near a magnetic cusp. The model was applied to the northern polar coronal hole of 1973 because observations provided a density distribution throughout the hole and showed that the hole was essentially axisymmetric (Munro and Jackson, 1977). The observed density was matched throughout the entire volume, and the observed geometry of the boundary was matched to a streamline, minimizing the impact of the polytrope assumption. The results are shown in Figures 1 and 2. Important deductions include an "effective" temperature of $1-2 \times 10^6$ deg., a field strength of 0.5 to 1.0 gauss, and a flow speed of a few up to 150 km/s at 2 solar radii. By 5 solar radii, the flow speed varies from less than 50 to over 300 km/s while the magnetic field is approximately uniform across the hole.

+Also, Department of Astro-Geophysics, University of Colorado,
Boulder, Colorado 80309.

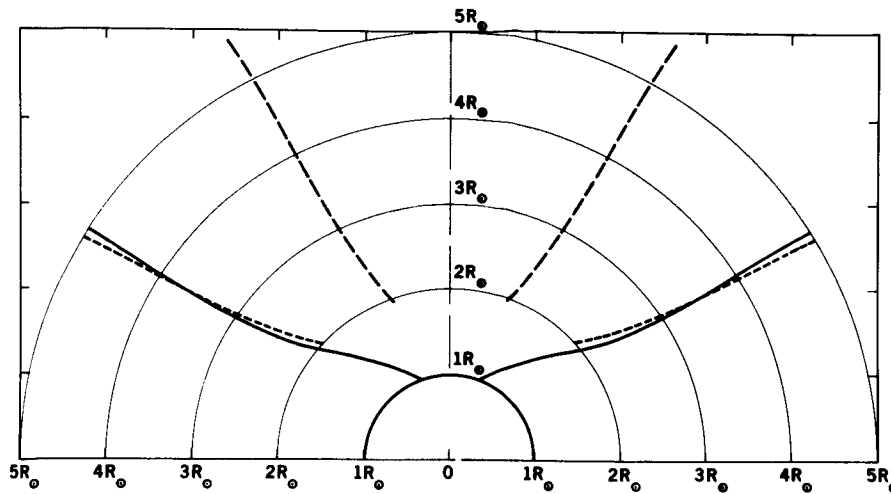


Figure 1. The observed boundary of the northern polar coronal hole (solid curve, from Munro and Jackson, 1977) and streamlines beginning at 2 solar radii and polar angles of 20 and 50 degrees. The streamlines have been computed using a quasi-radial approximation to the MHD equations of motion together with latitude dependent boundary conditions (from Suess, *et al.*, 1977).

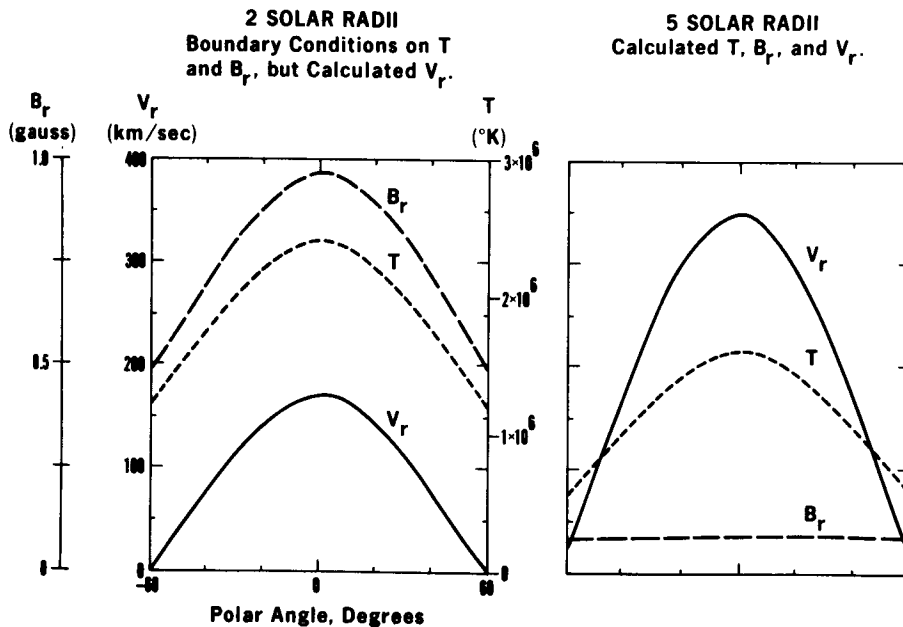


Figure 2. Latitudinal variations of the radial magnetic field, temperature and radial velocity at 2 and 5 solar radii. The radial magnetic field, temperature and observed density variation at 2 solar radii are the boundary conditions for this, and the streamline results in Figure 1 (Suess, *et al.*, 1977).

Significant energy deposition is implied between 2 and 5 solar radii. However, because this analysis cannot treat global flows that include regions of closed magnetic fields, it cannot be carried much beyond this particular example. The only obvious extensions would be to relax the polytropic assumption to permit thermal dissipation, and to include momentum and energy source terms.

In a corona with both closed, magnetostatic regions, and open, coronal-hole-like regions, the problem of the global gas-magnetic field interactions is both totally nonlinear and geometrically complex, almost requiring numerical solution. Probably the most pioneering work was that by Pneuman and Kopp (1971), who constructed a solution for an axisymmetric, isothermal streamer configuration on a two-dimensional grid. Their solution was found through a procedure which iterated on the current distribution, and they assumed isothermal flow.

The ultimate fieldline geometry computed by Pneuman and Kopp is shown in Figure 3. Originally, there were questions regarding their assumption about the nature of the cusp. However, these were laid to rest using a numerical solution of the time-dependent equations of motion (Endler, 1971; Weber, 1978). If the situation is treated as an initial-boundary value problem, then it is guaranteed that the final state is a true equilibrium configuration. In this approach, one starts with an initial state consisting of an essentially arbitrary choice for the fluid and magnetic field variables. The numerical solution of the time-dependent equations, starting with this non-equilibrium state, then gradually approaches a stationary coronal configuration. In applying this approach, it was not only shown that the cusp geometry assumed by Pneuman and Kopp was a valid equilibrium configuration, but also that the solution was stable.

These results demonstrated that treatment of steady, global coronal flow as an initial-boundary value problem is: (i) feasible, (ii) efficient, and (iii) probably the most powerful approach to the general problem. I would now like to describe results from an application of this approach to polytropic rather than isothermal flow, for a survey of the effect of varying magnetic field strength (Steinolfson, et. al., 1982).

THE PROBLEM AND THE EQUATIONS

The assumptions are that the corona can be described by polytropic, axisymmetric, single fluid flow. The initial state consists of a hydrodynamic solution to the steady radial equations of motion for a polytropic gas, superimposed on a dipole magnetic field. No explicit dissipation is included. This is a generalization over previous work by relaxing the assumption of isothermal flow. With these assumptions, the time-dependent equations of motion, in MKS units, are:

$$\frac{\partial \rho}{\partial t} + \frac{\partial}{\partial r}(\rho u) + \frac{\partial}{\partial \theta} \left(\frac{\rho v}{r} \right) = -\frac{2\rho u}{r} - \frac{\rho v}{r} \cot \theta, \quad (1a)$$

$$\begin{aligned} \frac{\partial u}{\partial t} + u \frac{\partial u}{\partial r} + \frac{B_\theta}{\mu\rho} \frac{\partial B_\theta}{\partial r} + \frac{1}{\rho} \frac{\partial p}{\partial r} + \frac{v}{r} \frac{\partial u}{\partial \theta} - \frac{B_\theta}{\mu\rho r} \frac{\partial B_r}{\partial \theta} \\ = -\frac{GM_s}{r^2} + \frac{v^2}{r} - \frac{B_\theta^2}{\mu\rho r}, \end{aligned} \quad (1b)$$

$$\begin{aligned} \frac{\partial v}{\partial t} + u \frac{\partial v}{\partial r} - \frac{B_r}{\mu\rho} \frac{\partial B_\theta}{\partial r} + \frac{v}{r} \frac{\partial v}{\partial \theta} + \frac{B_r}{\mu\rho r} \frac{\partial B_r}{\partial \theta} + \frac{1}{r\rho} \frac{\partial p}{\partial \theta} \\ = \frac{B_r B_\theta}{\mu r \rho} - \frac{uv}{r}, \end{aligned} \quad (1c)$$

$$\frac{\partial B_r}{\partial t} - \frac{\partial}{\partial \theta} \left(\frac{uB_\theta - vB_r}{r} \right) = \frac{1}{r} (uB_\theta - vB_r) \cot \theta, \quad (1d)$$

$$\frac{\partial B_\theta}{\partial t} + \frac{\partial}{\partial r} (uB_\theta - vB_r) = -\frac{1}{r} (uB_\theta - vB_r), \quad (1e)$$

$$\begin{aligned} \frac{\partial p}{\partial t} + \gamma p \frac{\partial u}{\partial r} + u \frac{\partial p}{\partial r} + \frac{\gamma p}{r} \frac{\partial v}{\partial \theta} + \frac{v}{r} \frac{\partial p}{\partial \theta} \\ = -\frac{\gamma p}{r} (2u + v \cot \theta), \end{aligned} \quad (1f)$$

where the dependent variables are the density, ρ , radial velocity, v_r , meridional velocity, v_θ , pressure, p , radial magnetic field, B_r and meridional magnetic field, B_θ . The independent variables are the radius, r , and the colatitude, θ . The constants are the polytropic index, γ , magnetic permeability, μ , universal gravitational constant, G , and the solar mass, M_s .

These equations are solved between 1.0 and 5.0 solar radii, and from the pole to the equator - the solution is symmetric about the equator. The grid spacing is 0.1 solar radii in the radial direction, 2.5 degrees in the meridional direction, the numerical solution uses a modified Lax-Wendroff differencing scheme, and the time step is chosen to be the maximum allowable from the usual stability criterion for dissipationless schemes; i.e.,

$$\Delta t = \min(\Delta t_r, \Delta t_\theta) \quad (2)$$

where

$$\Delta t_r = r/\lambda_r$$

and

$$\Delta t_\theta = r\theta/\lambda_\theta$$

and $(\lambda_r, \lambda_\theta)$ are the maximum eigenvalues (the sum of the fluid velocity and the characteristic velocity) in the radial and meridional directions. A smoothing term is used to reduce numerical oscillations, and it was necessary to watch for nonzero values of $\text{div} \cdot \underline{B}$ which otherwise often exist in numerical solutions of multi-dimensional time-dependent MHD problems (Brackbill and Barnes, 1980). At the inner boundary, two of the six radial characteristic directions are negative, and consequently, information from the region of interest propagates upstream to the boundary. In this case, four dependent variables at the lower boundary can be specified arbitrarily, and two must be calculated from some form of compatibility relations (Steinolfson and Nakaga-

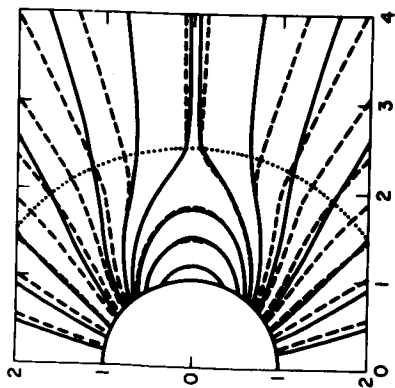


Figure 3. The coronal expansion calculation by Pneuman & Kopp (1971), compared to a potential field model (Newkirk, 1972).

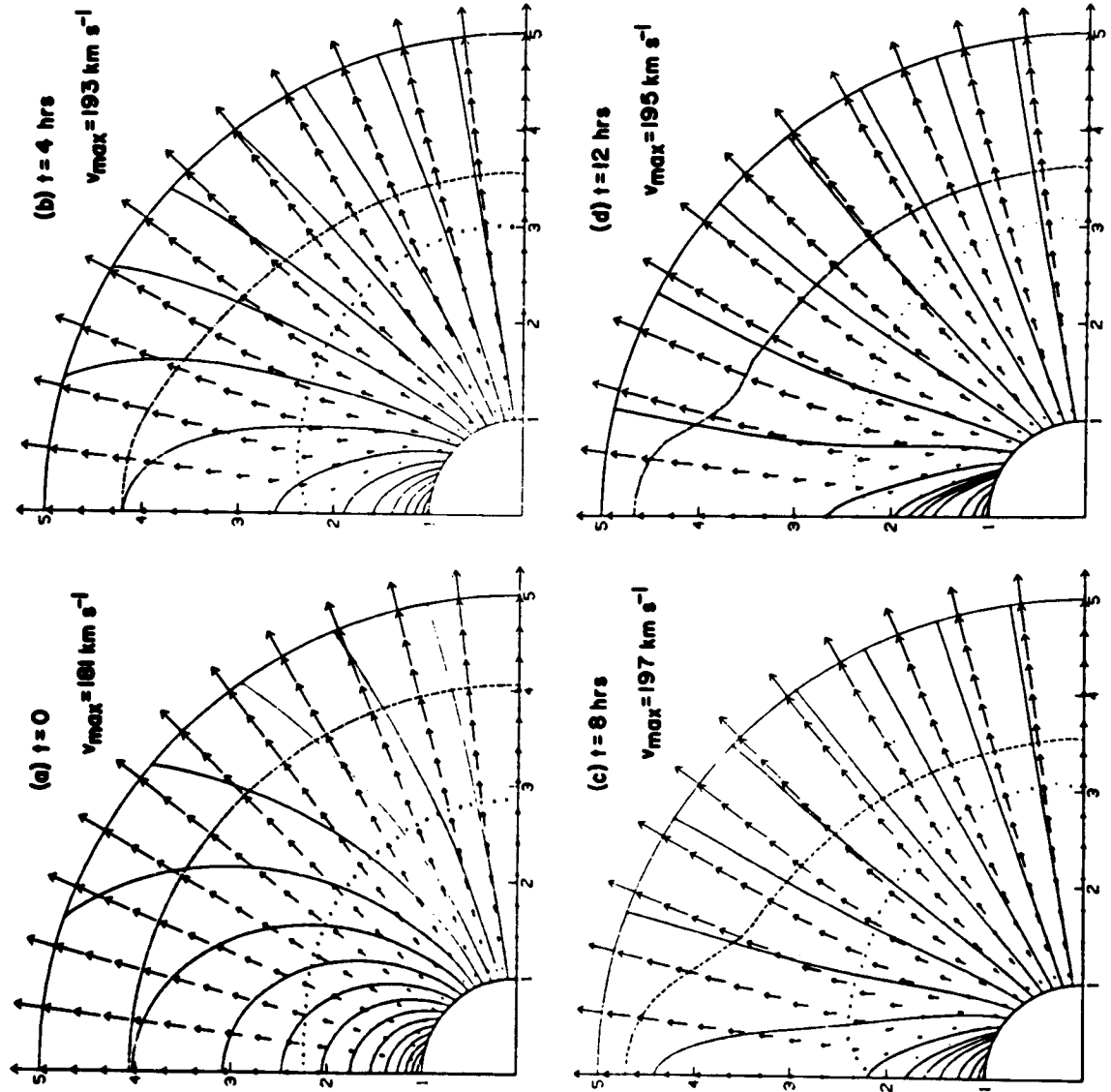


Figure 4. The evolution of the coronal magnetic field and velocity for $\beta = 0.5$. The sonic curve is the dashed line, the Alfvén curve is the dotted line, and the equator is the vertical axis. The velocity vectors point in the direction of the flow at their base, and their length is proportional to the velocity magnitude (Steinolfson, *et al.*, 1982).

wa, 1976). Strictly speaking, the compatibility relations are equations that can be derived from the equations of motion which must be satisfied by the dependent variables in each of the characteristic directions. Steinolfson and Nakagawa have shown that first-order or second-order (linear) extrapolation often works as well as using the more complex compatibility relations. Steinolfson, et. al used linear extrapolation to obtain the pressure and meridional magnetic field at the inner boundary. The radial magnetic field was held at its initial value so that the total magnetic flux through the solar surface remains constant. The radial velocity was also held constant with the exception that it could decrease to zero at the surface inside the closed field region. The meridional velocity was calculated so that the total velocity and magnetic field were parallel at the surface. The surface density was selected so that p/ρ^γ was constant.

In the initial state of spherically symmetric flow and a dipole potential field, the boundary values at 1 solar radius, and the system constants are:

$$T_o = 1.8 \times 10^6 \text{ degrees}$$

$$n_o = 2.25 \times 10^8 \text{ cm}^{-3}$$

$$\gamma = 1.05$$

$$\beta = \frac{2n_o k T_o}{B_o^2 / 8\pi} \quad (3)$$

$$B_o = |B| \text{ at 1 solar radius, at the equator.}$$

Using this definition of the plasma beta, results are summarized below for values of beta from 0.1 to 100. Values for the reference magnetic field of 0.83 G and 2.35 G at the equator yield values for the plasma beta of 4 and 0.5, respectively.

RESULTS: RELAXATION TO A STEADY STATE

Beginning with the previously stated initial configuration of a dipole potential field superimposed on a spherically symmetric flow, the relaxation then proceeds in time until the solution is approximately steady - meaning the solution did not change appreciably over a period of 2 hours. The intermediate states themselves have little physical meaning. However, the relaxation time to a steady state does have physical meaning - it is typical of the time the corona would take, given the assumptions of the model, to return to equilibrium after a large-amplitude perturbation. Figure 4 shows the evolution of the coronal magnetic field (solid lines) and velocity (vectors) for beta = 0.5. The initial state is in panel (a), and subsequent states at 4, 8 and 12 hours are shown in panels (b), (c) and (d) respectively. There is little change after 12 hours. It is easy to see the field lines evolving from a closed dipole field to a coronal streamer with the closed field lines lying

beneath and adjacent to open field lines. The dashed line is the sonic curve and the dotted line is the Alfvén curve. The sonic curve is displaced inwards in the final state, except for a small region around the equator, due to the general increase in the velocity. In the closed region, the pressure and density are increased over their initial values, and the velocity is approximately zero. Figure 5 shows cuts through the final configuration, at the pole and the equator. The high density and pressure in the closed region are evident, as is the zero velocity. Enhanced flow in the center of the open region is due essentially to the effects described by Kopp and Holzer (1976). However, the overall results are not exactly equivalent because they held the energy per gram, or flow speed infinitely far from the sun fixed, whereas here the boundary condition on temperature and velocity was held fixed on the sun. The Kopp and Holzer study dealt with the effects of changing "spreading factor" (overall flux tube divergence), whereas here a change in divergence occurs naturally along different streamlines.

Some of the effects of differing divergence can be simulated by changing the magnetic field strength. This was done by changing beta in steps from 100.0 to 0.1. Again, the results cannot be directly compared with those of Kopp and Holzer because the energy per gram at infinity is not a constant. The results from changing field strength are summarized in Figures 6 and 7. Figure 6, showing the maximum pressure and density in the closed region after scaling by the initial flow values, indicates the physical relevance of the beta parameter. The curves remain near a value of unity until $\beta < 1.0$. Then, they rise steeply for values of beta less than ca. 0.5. At the same time, there is a corresponding general increase in the height of the streamer. However, the width of the base of the streamer has only a weak dependence on beta.

Figure 7 shows the latitudinal variation of the pressure, density and temperature at five solar radii, for a range of beta on either side of unity. Again, these variables are scaled by their initial values. The velocity is shown in Figure 8. For values of $\beta \geq 1$, the only substantial effect is that the velocity is slightly depressed and the density is enhanced in the streamer. As beta is reduced below unity, a more rapid change begins to appear over the open region. Simultaneously, the velocity in the hole begins to increase rapidly, and the density and temperature begin to decrease. This is, in general terms, the same phenomenon observed by Kopp and Holzer (1976) and Steinolfson and Tandberg-Hanssen (1977), and is due to the divergence along a streamline being more than the underlying radius-squared divergence - which is commonly called a spreading factor of more than unity.

Note that the maximum velocity at 5 solar radii is not at the center of the hole, but instead near the edge at a polar angle of 60 degrees at 5 solar radii. This reflects a combination of the boundary condition on velocity being spherically symmetric, together with the overall spreading factor between 1 and 5 solar radii being dominated by potential field-like effects near the sun. The spreading factor is largest near the edge of the hole, although it is also larger than unity near the center of the hole. As beta decreases below unity, the increasing spreading factor causes the sonic critical point to begin moving rapidly inward (from 3.5 to 2.9 solar radii for beta decreasing from 0.5 to 0.1). As in earlier studies, the consequence is a rapid increase in local flow speed (but not the terminal flow speed), with the

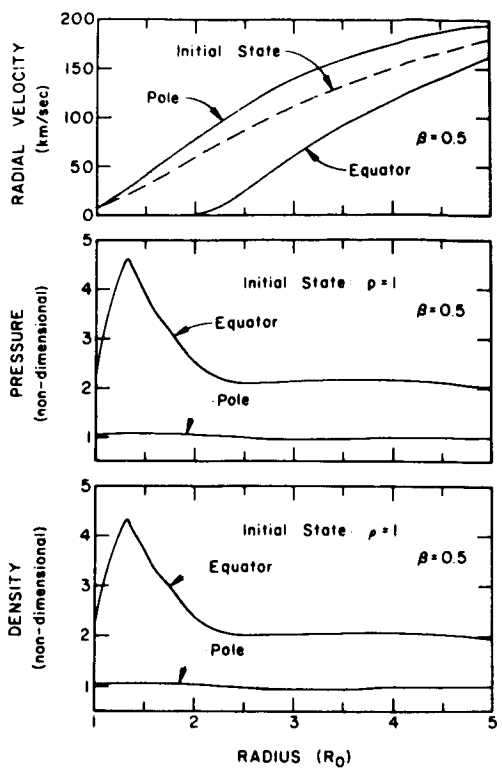


Figure 5. Radial distribution of the density, pressure and radial velocity initially (dashed line) and in the coronal streamer for beta = 0.5, at the pole and equator (Steinolfson, et al., 1982).

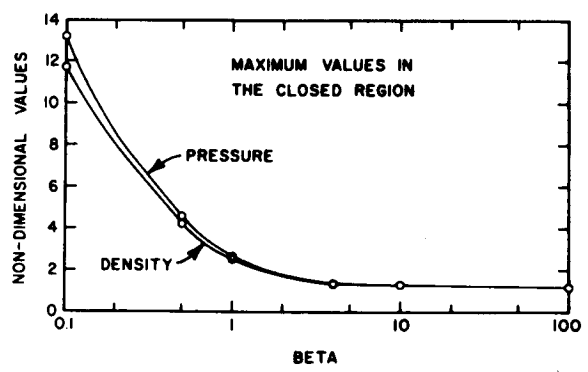


Figure 6. The dependence of the maximum pressure and density in the magnetically closed region on the reference beta (Steinolfson, et al., 1982).

largest increase occurring where the spreading factor is largest.

The result of this simulation and survey of magnetic field strength effects has been to produce a self-consistent streamer-coronal hole configuration. The streamer, in which the closed field region extends slightly more than 1 solar radius above the surface and whose width is somewhat less than the height, is quite similar to a typical streamer in its general features. The coronal hole is geometrically similar to, for example, the polar coronal hole observed during the Skylab period, and the density at the center of the hole is less than at the edges. However, there is good reason to believe the velocity should also increase towards the center of the hole (Suess, et. al., 1977). That it doesn't is due to the choice of boundary conditions and the lack of extended energy and momentum addition other than what is implicit in the polytrope formulation. The simulation shown in Figures 1 and 2 gave a detailed fit to the polar coronal hole data reported by Munro and Jackson (1977). There, it was shown that a large variation in density and temperature was required at the inner boundary - 2 solar radii - in order to fit the observations. In order to fit those data using the model of Steinolfson, et al., it would be necessary to invoke a corresponding variation at 1 solar radius, or to deposit energy into the flow between 1 and 2 solar radii. The conclusion then must be that to simulate at least one specific coronal hole, energy and momentum must be deposited in the flow between 1 and 2 solar radii because there is little evidence for the alternative possibility of significantly higher temperatures and densities beneath the hole, at the transition region level.

Before leaving this topic, there are two additional important specific results worth noting (R. S. Steinolfson, pers. comm.). First, there has been a question of whether the final configuration shown in Figure 4 is unique. To address this first question, Steinolfson began with an initial state that was radically different than that shown in Figure 4. It had the same spherically symmetric flow field, but now with a strictly radial magnetic field whose strength at the surface varied in the same way as the radial component of a dipole field. This exercise requires that field lines can "reconnect" as they are advected inward through the outer boundary in order to form the closed field region of the streamer. This is possible here not because ohmic diffusion is specifically included, but because there is sufficient numerical diffusion to allow a similar process to occur. The simulation produced exactly the same final configuration as was found when starting with a dipole potential field, so that the conclusion is: the present example has a unique solution. The second question has to do with the suggestion that standing shock waves may exist for certain ranges of spreading factor and initial conditions (Holzer, 1977; Habbal and Tsinganos, 1983). The study of Steinolfson, et al. cannot completely answer the question of whether these shocks ever actually occur in flows where the transverse pressure balance in the presence of a magnetic field is explicitly computed, because a beta of 0.1 is not sufficiently small to produce the extreme spreading factors invoked in some of those studies. However, these computations for beta between 100 and 0.1 are probably sufficient to cover most cases of relevance to the sun. Since no standing shocks were observed, it is suggested that the phenomenon may not be of importance in the solar atmosphere.

PROSPECT FOR FUTURE MODELING

The most interesting direction that can be taken in the development of numerical models of the steady corona would be to include a more detailed description of the energetics of the flow. The polytropic description is limited by many well known deficiencies. An obvious step would be to treat thermal conduction explicitly, and later to expand the calculation to deal with non-collisional forms of the conductive energy transfer. Other similar, but less important generalizations would be to include radiative losses and ohmic diffusion. For detailed models of specific observations, until the actual processes are discovered, it may also be necessary to include an empirical description of energy and momentum deposition. As stated earlier, the model described by Steinolfson, et al. used a modified Lax-Wendroff differencing scheme, which incorporates explicit time-differencing. Because of the Courant condition for stability on the maximum time-step, such models are effectively unuseable for calculations including thermal or ohmic diffusion because the maximum allowable time step decreases linearly with the largest characteristic speed. Literally thousands of time-steps would be required with thermal diffusion in order to do the analogous problem to the relaxation described earlier.

The alternative is to use implicit time-differencing which, although algebraically complex, is not limited by the Courant condition or round-off errors proportional to $(\Delta t/\Delta x)^2$ - as is the case with the Dufort-Frankel method (Richtmeyer & Morton, 1967). In fact, it is probable that these schemes would result in a considerable improvement in computational efficiency - even for the problem treated by Steinolfson, et al. The reason for this is that, because no particular physical interest exists for the intermediate steps between the arbitrary initial state and the final steady-state, time steps too large to resolve specific intermediate dynamic fluctuations can be used and still arrive at the desired final state. This is because the steady-state solution, if one exists, is found totally independent of the step size. The one qualification is that if multiple steady-state solutions exist, then there is the possibility that the solution that is actually realized will depend on the step size because a sufficiently large dynamic fluctuation can cause the asymptotic approach to a final solution to jump to an alternative branch.

To the best of my knowledge, no implicit scheme has been applied to the problem described by Steinolfson, et al. As a substitute, I will summarize the results from a prototype calculation on one-dimensional, transonic, thermally conductive flow (Suess, 1982), and outline how the analysis is extended to multi-dimensional magnetohydrodynamic flow. First, for the one-dimensional problem, the equations are:

$$\frac{\partial p}{\partial t} + \frac{1}{r^2} \frac{\partial}{\partial r} (r^2 \rho v_r) = 0, \quad (4a)$$

$$\rho \left(\frac{\partial v_r}{\partial t} + v_r \frac{\partial v_r}{\partial r} \right) = - \frac{\partial p}{\partial r} - \rho \frac{GM}{r^2}, \quad (4b)$$

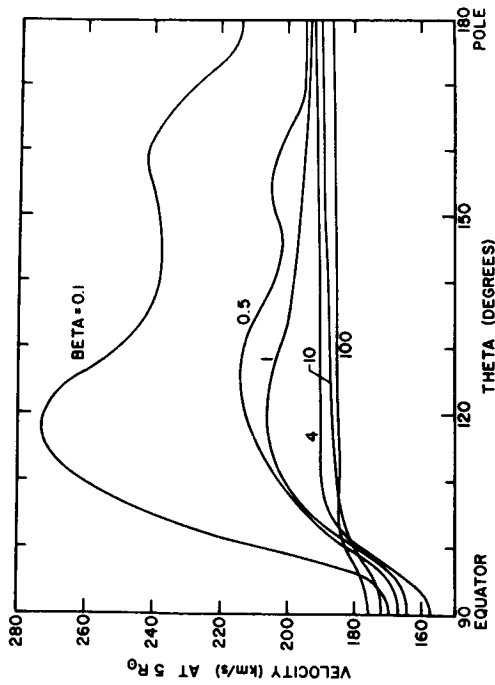


Figure 8. The meridional distribution of the radial velocity at 5 solar radii, as a function of the reference beta (Steinolfson, *et al.*, 1982).

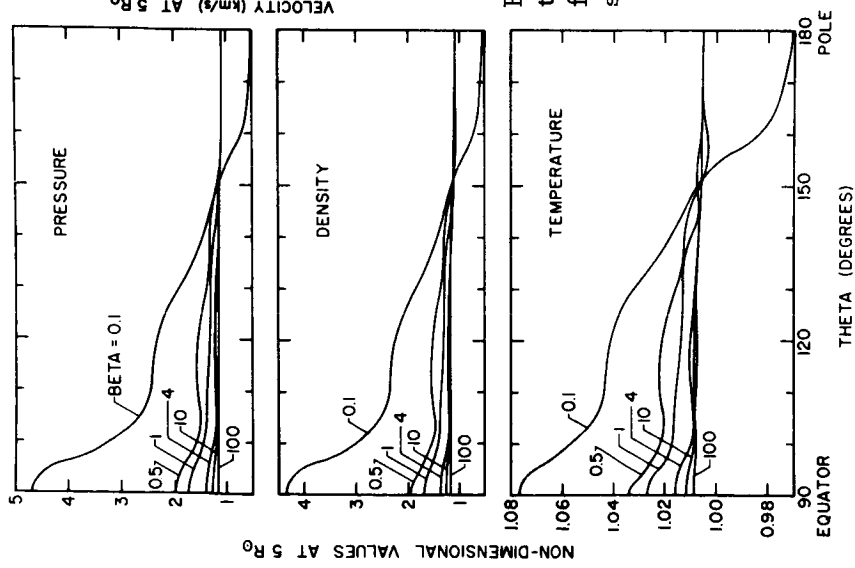


Figure 7. The meridional distribution of the thermodynamic variables at 5 solar radii, as a function of the reference beta. The variables are referenced to their initial values at 5 solar radii, before the relaxation (Steinolfson, *et al.*, 1982).

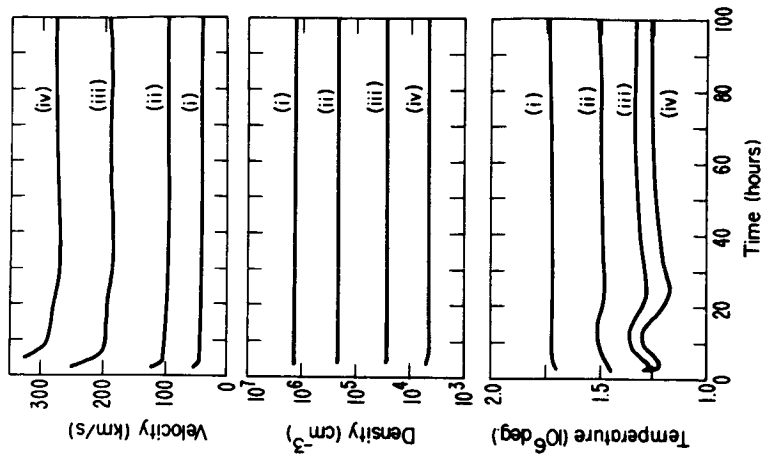


Figure 9. Relaxation from an initial state of isothermal flow to a final, thermally conductive, steady state. The curves begin at the third time step. In the plots for density, temperature and velocity, the curves labelled (i)-(v) are at 1.01, 1.51, 2.51, 5.12 and 10.24 solar radii, respectively.

$$\frac{\partial e}{\partial t} + \frac{1}{r^2} \frac{\partial}{\partial r} [r^2 v_r (e + p)] + \frac{1}{r^2} \frac{\partial}{\partial r} (r^2 q) + \rho v_r \frac{GM}{r^2} = 0, \quad (4c)$$

where ρ is the density, v_r is the radial velocity, p is the pressure, e is the total (kinetic plus internal) energy per unit volume, and M is the mass of the Sun.

$$p = 2nkT = 2\rho \left(\frac{k}{m_p + m_e} \right) T \equiv 2\rho RT,$$

$$R \approx 8.317 \times 10^7 \text{ (cgs).}$$

$$q = -\kappa T^{5/2} \frac{\partial T}{\partial r},$$

$$\kappa = \frac{1.99 \times 10^{-5}}{\ln \Lambda} \text{ (cgs),}$$

$$\Lambda \approx 1.246 \times 10^4 (T^3/n)^{1/2}.$$

The details of the calculation are described by Suess (1982). The solution uses three-level implicit time-differencing that is unconditionally stable for any time-step. Solutions are found on a variable temporal and spatial grid using a near-conservation form of the equations and occasionally with a small amount of artificial dissipation inserted in such a way as to preserve the formal accuracy of the differencing scheme. The spatial grid is not split, and the solution is fully implicit - treating all equations simultaneously. The algorithm uses a Taylor series expansion and Jacobian matrices to deal with nonlinear coefficients so that there is no iteration of any kind between time levels. Finally, although three levels in time are used, the algorithm requires only two levels to be stored - thereby minimizing memory requirements. The algorithm is applied here to a one-dimensional problem, but I will illustrate, in general terms, application to multi-dimensional problems after the example. The example is a demonstration of the efficiency of such algorithms on a classical problem. The initial state is isothermal solar wind flow with a temperature and density at 1 solar radius of 2×10^6 degrees and 10^{17} cm^{-3} respectively, resulting in a flow speed at 1 AU of ca. 400 km/s. Figure 9 shows the relaxation at several different radii, beginning with the third time-step. The time step is allowed to grow if the solution is changing sufficiently slowly. The relaxation proceeds rapidly at first, with some large oscillations and overshoot, settling down to a steady state inside 30 solar radii after 75-100 hours. The final time step was 22.2 hours and 19 steps were required for a total elapsed time of 108 hours.

The relaxation provides the correct, known solution and the relaxation time is essentially the advection time. This example is approximately equal

in computational efficiency to solving the steady-state equations in the standard way. As soon as an additional process such as radiative loss is introduced, the relaxation becomes the most efficient technique.

To indicate the procedure for multi-dimensional flow, I begin with the form of the time-differenced equations in the one-dimensional case:

$$L \left[\frac{\partial}{\partial r}, \frac{\partial^2}{\partial r^2} \right] \Delta U^n = F \quad (5)$$

where spatial differences have not yet been introduced, L is a matrix operator, ΔU^n is the vector of variables in conservation form - being the unknown at the next time step, and F is a matrix of known quantities at the present and previous time steps. Solution involves a matrix inversion or solution of a system of equations in order to find ΔU^n . In multiple dimensions, an approximate factorization can be made to give a corresponding equation of the form (for two dimensions):

$$L_1 \left[\frac{\partial}{\partial r}, \frac{\partial^2}{\partial r^2} \right] L_2 \left[\frac{\partial}{\partial \theta}, \frac{\partial^2}{\partial \theta^2} \right] \Delta U^n = F + \text{cross terms.} \quad (6)$$

which is solved in two steps:

$$L_1 \left[\frac{\partial}{\partial r}, \frac{\partial^2}{\partial r^2} \right] \Delta U^{n*} = F + \text{cross terms.}$$

$$L_2 \left[\frac{\partial}{\partial \theta}, \frac{\partial^2}{\partial \theta^2} \right] \Delta U^n = \Delta U^{n*}$$

That is, intermediate solutions are found by sweeping in one direction through the grid, at each time step, and the final solution for that time step is the produced by sweeping in the other direction through the grid. This is possible because the equation has been "factored" into operators depending on spatial gradients in only one direction. In the presence of magnetic fields, the factorization is not complete - some cross terms involving only the magnetic field remain. These cross terms are treated explicitly.

This factored implicit algorithm has been applied to a variety of ordinary hydrodynamic problems (Beam and Warming, 1976), with great success. It has been found generally to have superior stability limits and great flexibility. There is every reason to believe that it would work equally as well for determining steady-state structure in the corona.

CONCLUSION

I have described the approach to global modeling of the corona as an initial-boundary value problem in which the configuration is allowed to relax

in time from some initial state into a steady state. It is established that the technique is powerful, flexible and stable. The results include a survey of changing magnetic field strength effects and address questions about the uniqueness of the steady state and the possibility of standing shock waves. Application of advanced numerical methods now holds promise for being able to extend the present results by addressing the all-important problem of energy transfer in the corona, even in the presence of magnetic fields.

REFERENCES

- Beam, R. M., and Warming, R. F., An implicit finite difference algorithm for hyperbolic systems in conservation law form, J. Comput. Phys., 22, 87, 1976.
- Brackbill, J. U., and Barnes, D. C., The effect of nonzero $\text{div.}\mathbf{B}$ on the numerical solution of the magnetohydrodynamic equations, J. Comput. Phys., 35, 426, 1980.
- Endler, F., Ph.D. thesis, University of Gottingen, Germany, 1971.
- Habbal, S., and Tsinganos, K., Multiple transonic solutions with a new class of shock transitions in steady isothermal solar and stellar winds, J. Geophys. Res., 88, 1965, 1983.
- Holzer, T. E., Effects of rapidly diverging flow, heat addition, and momentum addition in the solar wind and stellar winds, J. Geophys. Res., 82, 22, 1977.
- Kopp, R. A., and Holzer, T. E., Dynamics of coronal hole regions, Sol. Phys., 49, 43, 1976.
- Munro, R. H., and Jackson, B. V., Physical properties of a polar coronal hole from 2 to 5 solar radii, Astrophys. J., 213, 874, 1977.
- Nerney, S. F., and Suess, S. T., Restricted three-dimensional stellar wind modelling. I. Polytropic case, Astrophys. J., 196, 837, 1975.
- Newkirk, G., Coronal magnetic fields and the solar wind, in Solar Wind, Proceedings of the Solar Wind Conference, Asilomar, Calif. (Sonett, Coleman & Wilcox, eds.), NASA Publication SP-308, p.11, 1972.
- Pneuman, G. W., and Kopp, R. A., Gas-magnetic field interactions in the solar corona, Sol. Phys., 18, 258, 1971.
- Richtmeyer, R. D., and Morton, K. W., Difference Methods for Initial Value Problems, Interscience, New York, 1967.
- Steinolfson, R. S., and Nakagawa, Y., Dynamical reponse of the solar corona. II. Numerical simulations near the Sun, Astrophys. J., 207, 300, 1976.
- Steinolfson, R. S., Suess, S. T., and Wu, S. T., The steady global corona, Astrophys. J., 255, 730, 1982.
- Steinolfson, R. S., and Tandberg-Hanssen, E., Thermally conductive flows in coronal holes, Sol. Phys., 55, 99, 1977.
- Suess, S. T., Three dimensional solar wind, J. Geophys. Res., 77, 567, 1972.
- Suess, S. T., Models of coronal hole flows, Space Sci. Rev., 23, 159, 1979.

- Suess, S. T., Unsteady, thermally conductive coronal flow,
Astrophys. J., 259, 880, 1982.
- Suess, S. T., Richter, A. K., Winge, C. R., and Nerney, S. F.,
Solar polar coronal hole - a mathematical simulation,
Astrophys. J., 217, 296, 1977.
- Weber, W. J., Ph.D. thesis, University of Utrecht, Holland, 1978.
- Winge, C. R., and Coleman, P. J., First order latitude effects
in the solar wind, Planet. and Space Sci., 22, 439, 1974.